2000-10

Estimating the Refractive Index Structure Parameter (Cn2) over the Ocean Using Bulk Methods

Frederickson, Paul A.; Davidson, Kenneth L.; Zeisse, Carl R.; Bendall, Charles S.

Journal of Applied Meteorology, Volume 39, October 2000, pp. 1770-1783.
https://hdl.handle.net/10945/41327

Estimating the Refractive Index Structure Parameter (C_n^2) over the Ocean Using Bulk Methods

PAUL A. FREDERICKSON AND KENNETH L. DAVIDSON

Department of Meteorology, Naval Postgraduate School, Monterey, California

CARL R. ZEISSE AND CHARLES S. BENDALL

Space and Naval Warfare Systems Center, San Diego, California

(Manuscript received 1 July 1999, in final form 2 December 1999)

ABSTRACT

Infrared scintillation measurements were obtained along a 7-km path over San Diego Bay concurrently with meteorological measurements obtained from a buoy at the midpoint of the path. Bulk estimates of the refractive index structure parameter C_n^2 were computed from the buoy data and compared with scintillation-derived C_n^2 values. The bulk C_n^2 estimates agreed well with the scintillation measurements in unstable conditions. In stable conditions the bulk C_n^2 estimates became increasingly higher than the scintillation values as the air–sea temperature difference increased. This disagreement may be due to enhanced wave-induced mixing of the lower atmosphere that decreases the vertical temperature and humidity gradients in stable conditions from the assumed Monin–Obukhov similarity (MOS) theory forms, resulting in bulk C_n^2 values that are too high. The bulk C_n^2 estimates decrease rapidly when the absolute air–sea temperature difference approaches small positive values. These predicted decreases in C_n^2 were not observed in either the path-averaged scintillation measurements or in single-point turbulence measurements, indicating that bulk models for estimating scalar structure parameters based on mean air–sea scalar differences are not valid when the mean air–sea difference approaches zero. The authors believe that the most promising means toward improving the bulk C_n^2 model is to obtain a better understanding of the MOS functions over the ocean for a wide stability range, and particularly of the role of ocean waves in modifying near-surface vertical gradients and turbulence characteristics.

1. Introduction

Electro-optical (EO) imagery through the atmosphere exhibits intensity fluctuations caused by atmospheric turbulence, a phenomenon known as scintillation. Scintillation is directly related to the refractive index structure parameter C_n^2; therefore knowledge of C_n^2 is essential to evaluate and to predict the effects of scintillation on EO imagery systems. Because direct measurements of C_n^2 are difficult to obtain, especially over the ocean, it is useful to be able to estimate C_n^2 from routinely measured environmental parameters. Bulk models have been developed to estimate atmospheric turbulence and gradient properties near the ocean surface from mean meteorological quantities (e.g., Fairall et al. 1996). The relations between these atmospheric properties and C_n^2 have also been established, thereby allowing near-surface C_n^2 values to be estimated from mean environmental measurements (e.g., Friehe 1977; Davidson et al. 1981; Andreas 1988; Claverie et al. 1995; Kunz et al. 1996; Tunick 1998; Forand 1999).

The goal of this study is to determine how accurately scintillation-derived C_n^2 values can be estimated over the ocean from routine meteorological measurements using bulk methods under a variety of environmental conditions. This study is based on data obtained during the Electro-Optical Propagation Assessment in a Coastal Environment (EOPACE) field experiments conducted in San Diego Bay in 1998. Bulk C_n^2 estimates computed from mean environmental measurements obtained on a buoy are compared with concurrent infrared scintillation-derived C_n^2 measurements along an overwater propagation path to determine how closely the two methods agree under various conditions.

2. The refractive index structure parameter C_n^2

For visible to near-infrared wavelengths λ, the refractive index for air n can be defined by the expression (Andreas 1988):

Corresponding author address: Mr. Paul A. Frederickson, Department of Meteorology, Naval Postgraduate School, 589 Dyer Rd., Room 254, Monterey, CA 93943-5114.
E-mail: pafreder@nps.navy.mil

$$n = 1 + 10^{-6}\left\{m_1(\lambda)\frac{P}{T} + [m_2(\lambda) - m_1(\lambda)]\frac{qP}{T\varepsilon\gamma}\right\}, \quad (1)$$

where P is the total atmospheric pressure (hPa), T is the absolute temperature (K), q is the specific humidity (g g^{-1}), ε is the ratio of the ideal gas constants for dry air over water vapor (=0.621 97), and $\gamma = (1 + 0.6078q)$. We have defined n in terms of *specific humidity* (mass of water vapor per mass of moist air) rather than *absolute humidity* (mass of water vapor per volume of moist air) because the bulk model used in this study is based on Monin–Obukhov similarity (MOS) theory, which is defined in terms of the conserved quantity specific humidity. The m_1 and m_2 functions in Eq. (1) are given by

$$m_1(\lambda) = 23.7134 + \frac{6839.397}{130 - \lambda^{-2}} + \frac{45.473}{38.9 - \lambda^{-2}} \quad (2)$$

and

$$m_2(\lambda) = 64.8731 + 0.580\,58\lambda^{-2} - 0.007\,115\,0\lambda^{-4} + 0.000\,885\,1\lambda^{-6}, \quad (3)$$

where λ is in micrometers. For the wavelength of interest in this study, 3.8 μm, $m_1 = 77.5$, and $m_2 = 64.9$.

Assuming pressure fluctuations are negligible, the turbulent fluctuation component of n can be expressed to a first-order approximation as (Andreas 1988):

$$n' = A(\lambda, P, T, q)T' + B(\lambda, P, T, q)q', \quad (4)$$

where a prime denotes the instantaneous turbulent fluctuation of a quantity about its mean value and the coefficients A and B are defined as

$$A = \frac{\partial n}{\partial T} = -10^{-6}\frac{P}{T^2}\left\{m_1(\lambda) + [m_2(\lambda) - m_1(\lambda)]\frac{q}{\varepsilon\gamma}\right\} \quad (5)$$

and

$$B = \frac{\partial n}{\partial q} = 10^{-6}[m_2(\lambda) - m_1(\lambda)]\frac{P}{T\varepsilon\gamma^2}. \quad (6)$$

In the inertial-subrange, the structure parameter for any quantity x is defined as

$$C_x^2 = \frac{\langle x'(0) - x'(d)\rangle^2}{d^{2/3}}, \quad (7)$$

where $x'(0)$ and $x'(d)$ are the turbulent fluctuation values of x at two points separated by a distance d in space and the angle brackets denote an ensemble average, which in practice is taken as a time average. The cross-structure parameter for any two quantities x and y can be defined similarly as

$$C_{xy} = \frac{\langle [x'(0) - x'(d)][y'(0) - y'(d)]\rangle}{d^{2/3}}. \quad (8)$$

By applying Eqs. (7) and (8) to Eq. (4) we can define the refractive index structure parameter C_n^2 in terms of the structure parameters for temperature, C_T^2, specific humidity, C_q^2, and the temperature-specific humidity cross-structure parameter, C_{Tq}, as follows (Andreas 1988):

$$C_n^2 = A^2C_T^2 + 2ABC_{Tq} + B^2C_q^2. \quad (9)$$

The first term on the right-hand side of Eq. (9) represents refractive index fluctuations caused by temperature fluctuations and is always positive, the second term represents the correlation of temperature and humidity fluctuations and can be positive or negative, while the third term represents humidity fluctuations and is always positive. As we shall see in section 5b, C_n^2 is an important quantity in EO propagation studies because it is a single parameter that quantifies image intensity fluctuations for a given path length and optical wavelength.

3. The bulk C_n^2 model

a. Monin–Obukhov similarity theory overview

Monin–Obukhov similarity theory can be used to relate C_n^2 to mean atmospheric surface layer properties. According to MOS theory, conditions are assumed to be horizontally homogeneous and stationary, and the turbulent fluxes of momentum, sensible heat, and latent heat are assumed to be constant with height in the surface layer. Scaling parameters for wind speed (u_*), temperature (T_*), and specific humidity (q_*) are defined in terms of the assumed-constant kinematic fluxes, as follows:

$$u_* \equiv \langle -w'u'\rangle^{1/2}, \quad (10a)$$

$$T_* \equiv -\frac{\langle w'T'\rangle}{u_*}, \quad \text{and} \quad (10b)$$

$$q_* \equiv -\frac{\langle w'q'\rangle}{u_*}, \quad (10c)$$

where u is the streamwise wind component and w is the vertical wind component.

According to MOS theory, any dynamic surface-layer property made dimensionless by the proper scaling parameters can be expressed as a universal function of ξ, defined as

$$\xi = \frac{zkg(T_* + 0.61Tq_*)}{\theta_v u_*^2}, \quad (11)$$

where z is the height above the surface, k is the von Kármán constant ($\approx$0.4), g is the gravitational acceleration, and θ_v is the virtual potential temperature. The mean vertical profiles of wind speed (U), temperature (T), and specific humidity (q) within the surface layer are defined according to MOS theory as follows:

$$U(z) = U_o + \frac{u_*}{k}\left[\ln\left(\frac{z}{z_{oU}}\right) - \Psi_U(\xi)\right], \quad (12a)$$

$$T(z) = T_o + \frac{T_*}{k}\left[\ln\left(\frac{z}{z_{oT}}\right) - \Psi_T(\xi)\right], \quad \text{and} \quad (12b)$$

$$q(z) = q_o + \frac{q_*}{k}\left[\ln\left(\frac{z}{z_{oq}}\right) - \Psi_q(\xi)\right], \quad (12c)$$

where the Ψ functions are the integrated forms of the respective dimensionless profile functions and are defined in the appendix. The ''roughness lengths'' z_{oU}, z_{oT}, and z_{oq} are the heights where the log-z profiles of U, T, and q, respectively, reach their surface values (denoted by the subscript ''o'') and are defined in section 3c below.

b. Structure parameter scaling

The structure parameters C_T^2, C_{Tq}, and C_q^2 can be expressed in terms of the surface layer scaling parameters as follows:

$$C_T^2 = T_*^2 z^{-2/3} f_T(\xi). \quad (13a)$$

$$C_{Tq} = r_{Tq} T_* q_* z^{-2/3} f_{Tq}(\xi), \quad \text{and} \quad (13b)$$

$$C_q^2 = q_*^2 z^{-2/3} f_q(\xi), \quad (13c)$$

where f_T, f_{Tq}, and f_q are empirically determined dimensionless functions and r_{Tq} is the temperature-specific humidity correlation coefficient. Recent measurements of f_T and f_q over the ocean in unstable conditions presented by Edson and Fairall (1998) are well described by the function

$$f_T(\xi) = f_q(\xi) = 5.9(1 - 8\xi)^{-2/3}, \qquad \xi \le 0. \quad (14)$$

In this study we use (14) for unstable conditions, and the stable function determined from the 1968 Kansas experiment (Wyngaard 1973), but with the modified multiplier 5.9, as follows:

$$f_T(\xi) = f_q(\xi) = 5.9(1 + 2.4\xi^{2/3}), \qquad \xi \ge 0. \quad (15)$$

The general form of this function has been confirmed by over-water measurements in near-neutral conditions presented by Edson et al. (1991). It should be noted that measurements of f_T and f_q in stable conditions generally exhibit much more scatter and are less common than in unstable conditions. Andreas (1988) and Hill (1989) have shown that following MOS theory to its logical conclusions demands that $f_T = f_{Tq} = f_q \equiv f$, as indicated by the Edson and Fairall (1998) measurements and others, therefore we have made this common assumption.

In the idealized case of a homogeneous and passive surface, MOS theory demands that $r_{Tq} = \pm 1$ (Hill 1989). For flows over real nonpassive surfaces such as the ocean with heterogeneous and nonidentical sources and sinks of heat and humidity, r_{Tq} values fall in the range $-1 < r_{Tq} < 1$, as confirmed by numerous experiments. Because the proper sign for C_{Tq} is determined by the product $T_* \times q_*$ in Eq. (13b), we are only concerned here with the absolute value of r_{Tq}. Measurements over both water (Fairall et al. 1980) and land surfaces (Kohsiek 1982; Andreas 1987; Andreas et al. 1998) indicate that for positive Bowen ratio values $r_{Tq} \approx 0.8$. For negative Bowen ratios, $|r_{Tq}|$ appears to have a lower value closer to 0.5 (Fairall et al. 1980; Andreas et al. 1998). The Bowen ratio is defined as the ratio of the sensible heat flux over the latent heat flux, and for our bulk model the sign of the Bowen ratio is given simply by the ratio $\Delta T/\Delta q$. Therefore, in this study we use a value of 0.8 for $|r_{Tq}|$ when $\Delta T/\Delta q > 0$, and 0.5 when $\Delta T/\Delta q < 0$. In section 4 we will see that the value used for r_{Tq} has a significant impact on the resulting C_n^2 estimates only for small $|\Delta T|$ values.

We can express C_n^2 in terms of mean meteorological properties by solving Eq. (12) for the scaling parameters u_*, T_*, and q_* and combining with Eqs. (9), (11), and (13), resulting in

$$C_n^2 = \frac{f(\xi)k^2(A^2\Delta T^2 + 2ABr_{Tq}\Delta T\Delta q + B^2\Delta q^2)}{z^{2/3}[\ln(z/z_{oT}) - \Psi_T(\xi)]^2}, \quad (16)$$

and

$$\xi = \frac{zg(\Delta T + 0.61T\Delta q)[\ln(z/z_{oU}) - \Psi_U(\xi)]^2}{\theta_v \Delta U^2[\ln(z/z_{oT}) - \Psi_T(\xi)]}, \quad (17)$$

where the Δ operator denotes a mean air–sea difference and we have assumed that $\Psi_q = \Psi_T$. Here, C_n^2 can be estimated by solving Eqs. (16) and (17) by an iterative process, once the roughness lengths are parameterized in terms of known quantities, as described in the next section.

c. Surface parameterization

The momentum roughness length z_{oU} can be parameterized as (Fairall et al. 1996):

$$z_{oU} = \frac{\alpha u_*^2}{g} + \frac{0.11\nu}{u_*}, \quad (18)$$

where ν is the kinematic viscosity of air and α is Charnock's parameter, which is thought to depend upon such factors as wave age, fetch, water depth, and so on, although the exact relationships are not clear. We have used a value of 0.0185 for α, as determined by Wu (1980) from measurements at a coastal location with a water depth similar to that of the present experiment. Use of such a constant value for α implicitly assumes that the wave field is fully developed (i.e., in equilibrium with the wind and hydrographic conditions).

Observations have indicated that the scalar roughness lengths behave quite similarly, therefore we assume $z_{oT} = z_{oq}$. The thermal roughness length z_{oT} can be parameterized as (Liu et al. 1979, hereinafter referred to as LKB):

$$z_{oT} = R_T \frac{\nu}{u_*}, \tag{19}$$

where R_T is the roughness Reynolds numbers for temperature. In the LKB model R_T is parameterized in terms of the roughness Reynolds number for wind speed, $R_U = z_{oU}u_*/\nu$. We propose the following function for R_T:

$$R_T = 5.4R_U^{4/3}(1.75R_U + 1)^{-2}. \tag{20}$$

Equation (20) is simpler to implement than the LKB functions, and, unlike the LKB model, is a smooth function with no first-order discontinuities.

The specific humidity at the surface q_o is determined by assuming the sea surface is saturated, therefore, $q_o = 0.98q_{\text{sat}}(T_o)$, where $q_{\text{sat}}(T_o)$ is the saturation specific humidity at the sea surface temperature T_o, and the factor 0.98 accounts for salinity effects. The wind speed at the ocean surface is assumed to be zero ($U_o = 0$). We have adopted the ''free-convective'' parameterization described by Fairall et al. (1996), in which U includes a ''gustiness'' component when $\xi < 0$, as follows:

$$U = (u_{\text{avg}}^2 + w_g^2)^{1/2}, \tag{21}$$

where u_{avg} is the scalar-averaged wind speed and w_g is the ''convective gustiness velocity'' given by

$$w_g = \beta\left[-\frac{gz_i u_*}{\theta_v}(T_* + 0.61Tq_*)\right]^{1/3}. \tag{22}$$

Here, β is an empirical constant with a value of about 1.25, and z_i is the convective boundary layer height, which we assume to be 600 m, as recommended by Fairall et al. (1996).

4. Analysis of the bulk C_n^2 model

In this section we examine the behavior and sensitivity of the bulk C_n^2 model upon assumed model parameters and input data and also discuss the possible sources of error in the model. First, the dependence of bulk C_n^2 estimates upon the value used for r_{Tq} is demonstrated. In Fig. 1 bulk log(C_n^2) values are plotted versus the air–sea temperature difference (ΔT) for different assumed relative humidity and r_{Tq} values. The C_n^2 values asymptote toward zero for all relative humidity curves when $r_{Tq} = 1$, while for $r_{Tq} = 0.8$ the C_n^2 values asymptote toward zero only when the relative humidity is 98%. By examining Eq. (16) we can see that using $r_{Tq} = 1$ allows C_n^2 to become zero when $\Delta T = -\Delta qB/A$, while assuming $r_{Tq} < 1$ allows C_n^2 to become zero only when $\Delta T = \Delta q = 0$. From Fig. 1 we can see that assuming $r_{Tq} < 1$ causes an increase in the resulting minimum C_n^2 values for each relative humidity curve and moves the C_n^2 minimum to slightly smaller values of ΔT. The increase in the C_n^2 minimum when using $r_{Tq} < 1$ becomes larger with decreasing relative humidity. Therefore, the value used for r_{Tq} has the greatest effect on the resulting bulk C_n^2 estimates for small positive values of ΔT and low relative humidity. In the following figures we use a value of 0.8 for r_{Tq} when $\Delta T/\Delta q > 0$, and a value of 0.5 when $\Delta T/\Delta q < 0$, as discussed in section 3b.

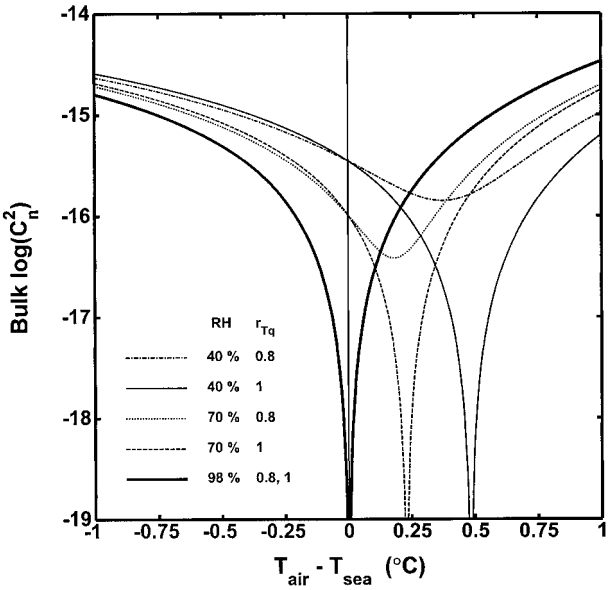

FIG. 1. Bulk log(C_n^2) estimates for different values of relative humidity (RH) and temperature-specific humidity correlation coefficient (r_{Tq}) as indicated, vs air–sea temperature difference. The bulk C_n^2 estimates were computed for wind speed = 5 m s^{-1}, sea temperature = 16°C, height above the surface = 5 m, and wavelength = 3.8 μm.

The dependence of the bulk C_n^2 estimates upon ΔT is shown for different wind speeds in Fig. 2, and for different relative humidity values in Fig. 3. From these

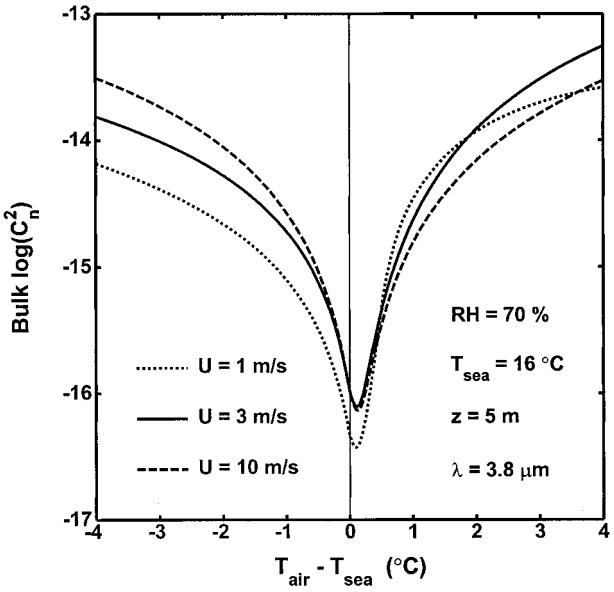

FIG. 2. Bulk log(C_n^2) estimates for different wind speeds (U) as indicated, vs air–sea temperature difference. The bulk C_n^2 estimates were computed for relative humidity = 70%, sea temperature = 16°C, height above the surface = 5 m, and wavelength = 3.8 μm.

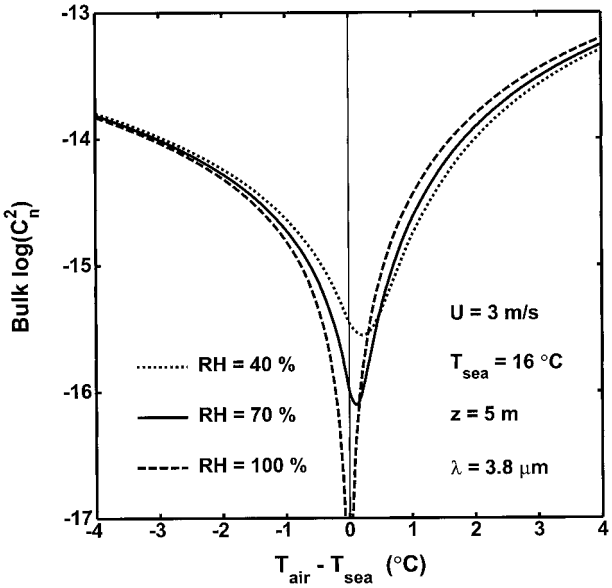

FIG. 3. Bulk log(C_n^2) estimates for different values of RH as indicated, vs air–sea temperature difference. The bulk C_n^2 estimates were computed for wind speed = 3 m s^{-1}, sea temperature = 16°C, height above the surface = 5 m, and wavelength = 3.8 μm.

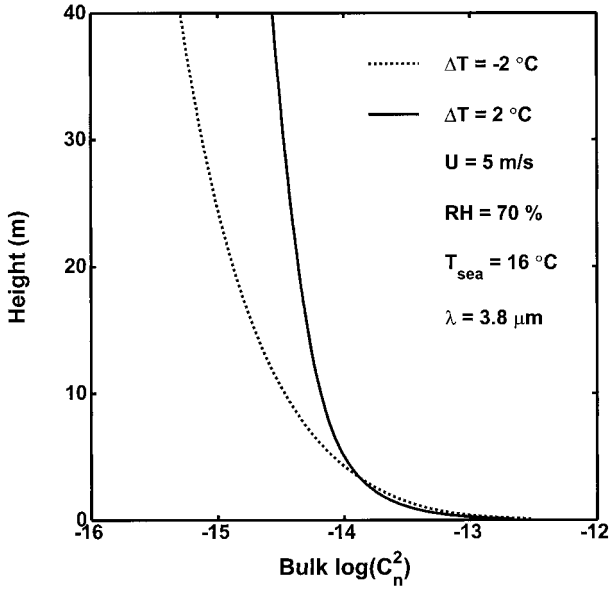

FIG. 4. Bulk log(C_n^2) estimates for different air–sea temperature differences (ΔT), as indicated, vs height above the surface. The bulk C_n^2 estimates were computed for wind speed = 5 m s^{-1}, relative humidity = 70%, sea temperature = 16°C, and wavelength = 3.8 μm.

figures we can see that the bulk C_n^2 estimates generally increase as $|\Delta T|$ increases, except for small positive values of ΔT depending upon the relative humidity. Variations in wind speed affect the bulk C_n^2 estimates by changing the magnitude of ξ, and thus $f(\xi)$. From Fig. 2 we can see that the C_n^2 estimates increase with wind speed when $\Delta T < 0$, and, except for small positive ΔT values and low wind speeds at higher ΔT values, decrease with wind speed when $\Delta T > 0$. The effects of wind speed variations on the resulting C_n^2 estimates are greatest for large $|\Delta T|$ values. From Fig. 3 we can see that the bulk C_n^2 estimates decrease with relative humidity when $\Delta T < 0$, and, except for small positive ΔT values, increase with relative humidity when $\Delta T > 0$. The minimum bulk C_n^2 value for each relative humidity curve increases and occurs at larger ΔT values as the relative humidity decreases. The effects of relative humidity variations on the resulting C_n^2 estimates are largest for small $|\Delta T|$ values.

Asymptotic scaling predicts that C_n^2 should decrease with height as $z^{-4/3}$ in the unstable limit ($\xi \to -\infty$) and as $z^{-2/3}$ in neutral conditions ($\xi = 0$), and should be constant with height in the stable limit ($\xi \to \infty$) (Wyngaard 1973). Figure 4 shows an example of the dependence of the bulk C_n^2 estimates on the height above the surface for unstable ($\Delta T = -2$°C) and stable ($\Delta T = 2$°C) conditions. In both cases C_n^2 decreases with height very rapidly in the lowest 5 m above the surface. The C_n^2 profile for positive ΔT values initially has a larger gradient with height near the surface and then becomes less dependent on height than the negative ΔT profile, as predicted.

The accuracy of the bulk C_n^2 model is dependent upon the validity of each assumption incorporated into the model, as well as upon the quality of the input data. Possible sources of error in a bulk C_n^2 estimate for any given situation include the following.

1) Traditional MOS theory, upon which the bulk model is based, is not valid because
   a) the relevant dynamical surface layer properties depend upon additional parameters beside u_*, T_*, q_*, z, and g/θ_v (such as sea state or wave age, fetch, internal boundary layer height, etc.);
   b) the turbulent fluxes are not constant with height; and
   c) conditions are nonstationary and/or nonhorizontally homogeneous.
2) The surface wave field is not fully developed (i.e., not in equilibrium with the wind field and hydrographic conditions), as implicitly assumed by using a constant Charnock parameter value.
3) There is uncertainty in the empirically determined model parameters and functions (i.e., k, r_{Tq}, α, β, Ψ, f_T, R_T, etc.).
4) There are measurement errors in the model input parameters (i.e., mean wind speed, air and sea temperature, relative humidity, and atmospheric pressure measurements).

It should be stressed that the bulk model presented here is formulated to describe C_n^2 as defined by Eq. (7) (where $x = n$), which is a statistical representation of refractive index fluctuations at essentially a single point in space and over a given averaging interval. The C_n^2 values determined from optical scintillation measure-

ments (see section 5b), on the other hand, are statistical representations of the fluctuations in image intensity caused by atmospheric turbulence and varying refractive, scattering, and absorption effects along a propagation path. Deviations between scintillation-derived C_n^2 measurements and bulk C_n^2 estimates are to be expected because of differences inherent to the nature of these two quantifies and the measurements used to determine them (i.e., path-averaged optical turbulence versus mean single-point environmental measurements). Factors leading to such differences may include, but certainly are not limited to

1) horizontally heterogeneous and nonstationary refractive conditions that cause EO rays to propagate at varying heights above the surface and possibly at a different height than assumed for the corresponding bulk C_n^2 estimation,
2) temporal and spatial aerosol concentration fluctuations along the propagation path that cause varying absorption and scattering characteristics that modify the measured intensity variances from those expected in a particle-free atmosphere (Sadot and Kopeika 1992), or
3) horizontal advection, internal boundary layer formation, surface roughness variations, and other processes that can cause varying refractive and turbulence characteristics along the propagation path and also can modify these properties from the MOS predictions used in the bulk model.

The factors listed here are expected to lead to larger variations in scintillation C_n^2 values as compared with bulk estimates because these effects are outside the scope of MOS theory and cannot be taken into account by the bulk model.

As pointed out above, the bulk model assumes stationary and horizontally homogeneous conditions and a fully developed wave field. These assumptions are most likely to be valid in open ocean regions. In coastal locations, offshore advection can lead to nonstationary and horizontally heterogeneous conditions and short fetch and shoaling effects can prevent the wind/wave fields from reaching equilibrium states (e.g., Anctil and Donelan 1996; Vickers and Mahrt 1997). For example, a recent study in a coastal zone by Mahrt et al. (1998) indicates that the heat flux can be significantly reduced from MOS predictions by the formation of internal boundary layers in offshore flow, especially for unstable conditions. Vickers and Mahrt (1999) found that internal boundary layer formation and growing wave fields in short-fetch conditions can lead to significant departures in the dimensionless wind profile from the traditional MOS theory based on stability alone. Despite such potential problems, we apply the MOS-based bulk model in a coastal location in this study, while keeping in mind the factors cited above.

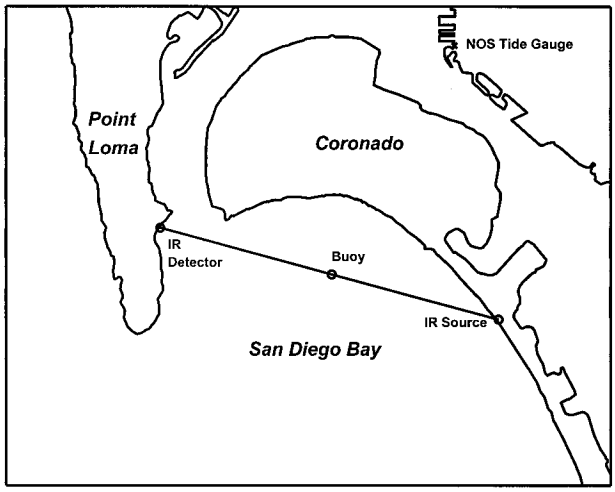

FIG. 5. Map of the EOPACE experiment area in San Diego Bay, showing the optical propagation path and the locations of the IR receiver and transmitter, the NPS buoy, and the NOS tide gauge.

5. The experiment

a. Buoy measurements

An instrumented buoy was deployed in San Diego Bay by the Department of Meteorology, Naval Postgraduate School (NPS) during experiments conducted in May–June and September 1998. The buoy was located at the midpoint of a 7-km propagation path (see Fig. 5), along which concurrent scintillation measurements were obtained, as described in the next subsection. The mean water depth at the buoy location was 8 m. Wind speed and direction were measured by a sonic anemometer (Vaisala, Inc., Handar Model 425) mounted 4.9 m above the buoy waterline. An onboard compass measured the buoy heading, enabling the wind direction relative to true north to be determined. Air temperature and relative humidity were measured by a Rotronics, Inc., MP101A sensor located within a forced-aspirated radiation shield mounted 3.55 m above the surface. The bulk sea temperature within several centimeters of the surface was measured by a thermistor placed within a float attached alongside the buoy hull. Atmospheric pressure was measured by an A.I.R. barometer. All of the above measurements were sampled at a 1-Hz rate. During postprocessing these data were averaged over 10-min intervals centered around the scintillation measurement times and bulk C_n^2 estimates were computed from these mean values. Because C_n^2 is height dependent, the bulk C_n^2 estimates were adjusted for tidal sea level variations using tide data obtained from the National Ocean Service (NOS) acoustic tide gauge located in San Diego Harbor (see Fig. 5). Assuming a straight-line path between receiver and detector, the infrared rays passed 4 m above mean sea level (MSL) at the buoy location. Therefore, the bulk C_n^2 estimates were computed for a height of 4 m minus the tide level variation from MSL.

High-frequency (21 Hz) wind and sonic temperature

measurements were obtained from a Solent sonic anemometer mounted atop the buoy mast at a height of 5.25 m above the waterline. The sonic temperature data were corrected for cross-path velocity contamination, as described by Fairall et al. (1997). Power spectral densities of the sonic temperature $S_{T_s}(f)$ were computed from successive 1024-data-point blocks (48.8 s duration) and were averaged in frequency bins over 10-min intervals. The sonic temperature structure parameter $C_{T_s}^2$ was then computed as follows:

$$C_{T_s}^2 = 4\left(\frac{2\pi}{U}\right)^{2/3} S_{T_s}(f) f^{5/3}, \tag{23}$$

where U is the mean wind speed and f is the frequency. Direct turbulent estimates of C_n^2 were obtained from the relation $C_n^2 = A^2 C_{T_s}^2$, which assumes that humidity fluctuation effects on both $C_{T_s}^2$, and C_n^2 are negligible compared to temperature fluctuations. This assumption is valid for large Bowen ratio values, when the temperature fluctuations are much larger than humidity fluctuations. Therefore, we assume the sonic-derived C_n^2 values are valid only when the absolute value of the bulk Bowen ratio is greater than 1.

b. Infrared scintillation measurements

The Space and Naval Warfare System Center, San Diego (SSC SD) measured scintillation across San Diego Bay concurrently with the NPS buoy environmental measurements. The scintillation measurements were obtained from 22 May to 14 June 1998 (yeardays 142 to 165) during the first experiment and from 2 to 21 September 1998 (yeardays 245 to 264) during the second. Scintillation was measured by recording the fluctuations in a midwave infrared signal transmitted across San Diego Bay (see Fig. 5). The transmitter, a 20-cm diameter F/6 Newtonian telescope, was mounted 5 m above MSL at the Naval Amphibious Base, Coronado. The receiver, an identical telescope, was mounted 4.9 m above MSL at the Naval Submarine Base, Point Loma. The receiver was 7.0 km distant from the transmitter on a bearing of 261° true.

The transmitter contained a 1200-K blackbody whose radiation was collected by a 20-cm diameter parabolic mirror and projected toward the receiver within a cone of angular width 5.4 mrad (full angle). At the receiver an identical mirror projected the arriving radiation onto a ZnSe lens that produced a collimated beam falling on a 2-mm diameter InSb detector. The receiver field of view was 5 mrad (full angle). The detector was covered with a cold optical filter with a nominally square passband from 3.52 to 4.12 μm. The detector was followed by a preamplifier and a phase-sensitive detector whose output was sampled at 400 Hz by a 12-bit analog-to-digital converter. The detector responsivity was 2.9 A W^{-1} and the in-phase detector noise was 3.5 pA $Hz^{-1/2}$ (limited by pickup). The equivalent noise bandwidth of the electronic system was 78 Hz. The detector noise and the analog-to-digital converter spacing were each 0.1% of the free-space detector signal, which was approximately 30 nA_{rms}. (The free space signal, which can loosely be thought of as ''100% transmission,'' is the signal that would be received in free space where there are no molecules, no aerosols, and all rays are straight.) Assuming a mean signal of 70% of free space (typical for clear air at this range), detector noise produced a normalized variance of 2×10^{-6}. Measurement techniques were identical during both experiments, except that in May–June 8192 consecutive samples (20.5 s duration) were acquired every 30 min whereas in September 32 768 consecutive samples (82 s duration) were acquired every 20 min.

The C_n^2 values were calculated from the normalized variance of the measured intensity fluctuations, σ_I^2, defined as

$$\sigma_I^2 = \frac{\langle I^2\rangle - \langle I\rangle^2}{\langle I\rangle^2}, \tag{24}$$

where I is a time series of intensity measurements and the angle brackets denote a time average. For a point source and small receiver and weak and isotropic turbulence conditions, σ_I^2 is given by the standard expression (e.g., Churnside 1993)

$$\sigma_I^2 = 0.496\kappa^{7/6} L^{11/6} C_n^2, \tag{25}$$

where κ is the optical wavenumber ($=2\pi/\lambda$), L is the path length, and Eq. (25) is valid for σ_I^2 less than about 1. This equation does not include the effects of aperture averaging resulting from the use of finite-size incoherent source and receiver apertures. To account for this effect we use the weak-turbulence equation given by Churnside (1993)

$$\sigma_I^2 = 16\pi^2\kappa^2 L \int_0^1 dr \int_0^\infty dK K \Phi_n \sin^2\left[\frac{K^2 L r(1-r)}{2\kappa}\right] \times \left\langle \left[\frac{2J_1(0.5KD_R r)}{0.5KD_R r}\right]\left[\frac{2J_1[0.5KD_T(1-r)]}{0.5KD_T(1-r)}\right]\right\rangle^2, \tag{26}$$

where J_1 is the Bessel function of the first kind, Φ_n is the refractive index spectrum, K is the turbulent wavenumber, r is the distance from the transmitter divided by the path length L, and D_R and D_T are the diameters of the receiver and transmitter, respectively. We have used a modified form of the Kolmogorov refractive index spectrum given by Churnside et al. (1992):

$$\Phi_n(K, C_n^2, l_o) = 0.033 C_n^2 K^{-11/3} \times \langle \exp(-1.28K^2 l_o^2) + 1.45\exp\{-0.97[\ln(Kl_o) - 0.45]^2\}\rangle, \tag{27}$$

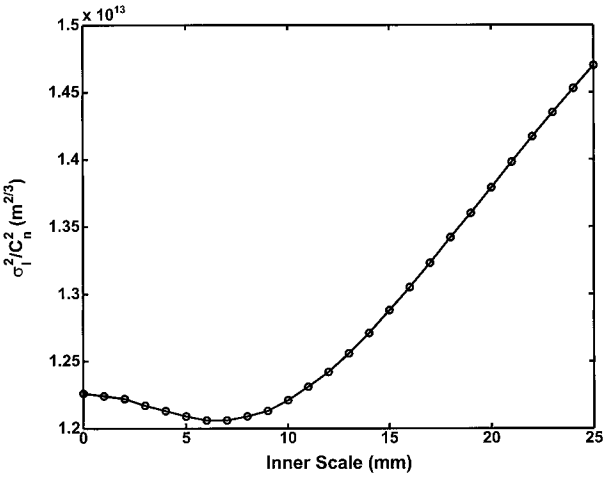

FIG. 6. The value $\tilde{\sigma}_I^2$ computed from Eqs. (33)–(35) for a wavelength of 3.8 μm, path length of 7 km, and source and receiver apertures of 20 cm vs the turbulent inner scale (l_o).

where l_o is the turbulence inner scale.

By inserting Eq. (27) into (26) and carrying out the double integration, we can write the following expression:

$$\tilde{\sigma}_I^2 = \frac{\sigma_I^2}{C_n^2} = 0.496\kappa^{7/6}L^{11/6}F(l_o, D_T, D_R). \qquad (28)$$

Here, $F(l_o, D_R, D_T)$ can be thought of as a dimensionless function that incorporates the effects of turbulence intensity (through l_o) and aperture averaging on σ_I^2. The $\tilde{\sigma}_I^2$ values computed for the experimental conditions ($\lambda = 3.8$ μm, $L = 7$ km, $D_R = D_T = 20$ cm) are plotted versus l_o in Fig. 6, which demonstrates that $\tilde{\sigma}_I^2$ varies by only about 20% over the range $0 \leq l_o \leq 25$ mm. This variation is small when we consider that σ_I^2 was observed to have values ranging over several orders of magnitude during the experiment (roughly 10^{-3} to 10^{0}). The l_o values were estimated from the buoy sonic anemometer wind turbulence data using the expression given in Hill and Clifford (1978). The buoy l_o measurements were in the range 5–25 mm, therefore, we have simply assumed a constant median value of 15 mm for l_o, resulting in $\tilde{\sigma}_I^2 = 1.288 \times 10^{13}$. For the case of infinitesimally small source and receiver apertures and small inner scale given in Eq. (25) [i.e., $F(l_o, D_R, D_T) = 1$], $\tilde{\sigma}_I^2 = 9.991 \times 10^{13}$. Therefore, the 20-cm transmitter and receiver apertures used in this experiment result in a reduction of σ_I^2 by a factor of 9.991/1.288 = 7.757, which incurs the advantage of increasing the range of C_n^2 values for which the weak-turbulence theory is valid ($\sigma_I^2 < 1$). As stated above, the normalized variance due to detector noise was about 2×10^{-6}, therefore the minimum detectable C_n^2 value with the current equipment is roughly 1.6×10^{-19} m$^{-2/3}$, which is about three orders of magnitude below the lowest observed C_n^2 values during the experiment of about 1×10^{-16} m$^{-2/3}$.

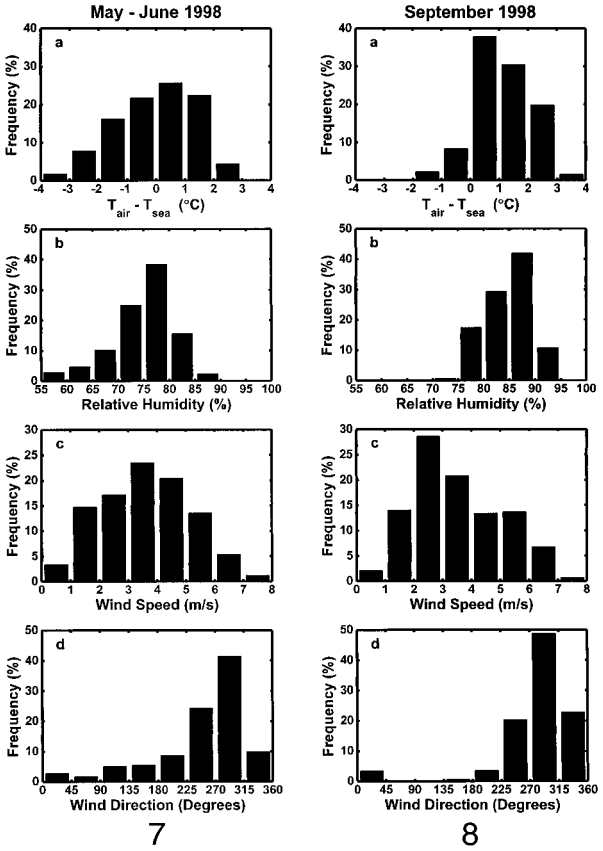

FIGS. 7 and 8. Frequency-of-occurrence histograms for meteorological observations from the NPS buoy during the May–Jun 1998 experiment in Fig. 7, and the Sep 1998 experiments in Fig. 8: (a) air–sea temperature difference, (b) relative humidity, (c) wind speed, and (d) wind direction.

The integral over r in Eq. (26) represents a spatial weighting function for σ_I^2 along the propagation path. Because the receiver and transmitter aperture diameters were identical in this experiment, the spatial weighting function is symmetrical about the maximum value at the midpoint of the propagation path and tapers to negligible values near the end points of the path (e.g., Wang et al. 1978). This weighting function was beneficial in minimizing beach effects and flow distortion around the receiver and transmitter housings at both ends of the path on the optical turbulence measurements. The center-path position of the NPS buoy was chosen to correspond to the maximum weighting location for the scintillation measurements.

6. Results

Mean environmental measurements from the NPS buoy are summarized as histogram plots in Fig. 7 for the May–June 1998 experiment and Fig. 8 for the September 1998 experiment. Atmospheric conditions were warmer and more humid on average during September, leading to larger values of ΔT and Δq as compared with

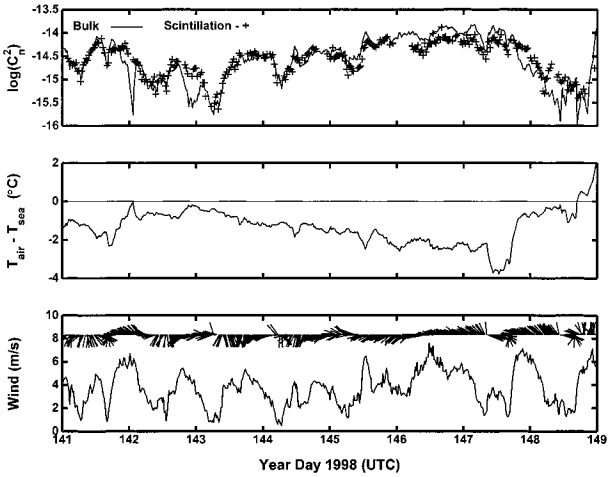

FIG. 9. Time series data for yeardays 141–148 (21–28 May) 1998 (UTC). (top) Bulk log(C_n^2) estimates indicated by solid line; scintillation log(C_n^2) measurements indicated by crosses (+). (center) Air–sea temperature difference measured on NPS buoy indicated by solid line. (bottom) Wind speed measured on NPS buoy indicated by solid line; wind direction with respect to true north indicated by barbs pointing into direction from which wind is blowing.

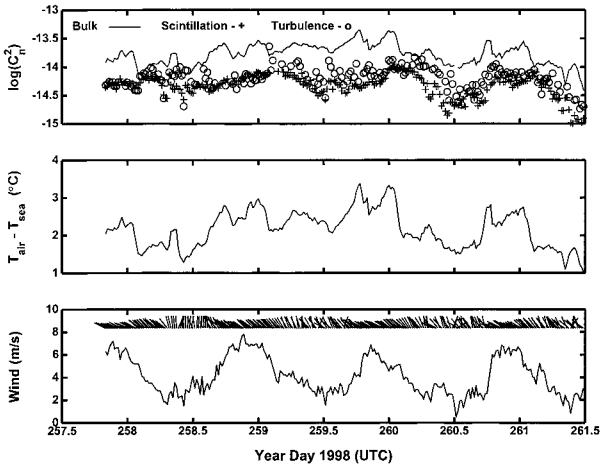

FIG. 10. Time series data for yeardays 257.5–261.5 (1200 UTC 14 Sep–1200 UTC 21 Sep 1998). (top) Bulk log(C_n^2) estimates indicated by solid line, scintillation log(C_n^2) measurements indicated by crosses (+), and buoy turbulent log(C_n^2) measurements indicated by circles (○). (center) Air–sea temperature difference measured on NPS buoy indicated by solid line. (bottom) Wind speed measured on NPS buoy indicated by solid line; wind direction with respect to true north indicated by barbs pointing into direction from which wind is blowing.

the May–June experiment. The wind speed was on average slightly higher during the May–June experiment, although winds never exceeded 8 m s^{-1} in either case. The wind directions were also quite similar for both experiments, with winds from the southwest through north (225°–360°) being most common. Therefore, much of the time the winds were from the direction of Point Loma (see Fig. 5) and closely paralleling the axis of the propagation path (284°).

A total of 41 days of data were collected during the two experiments. To conserve space only one representative time series plot is shown from each experiment. A time series for 21–27 May 1998 (yeardays 141–148) is presented in Fig. 9. No turbulent C_n^2 measurements were available during this period. Conditions were unstable through almost the entire period, with ΔT varying between about $-0.1°$ and -3.7°C, except for the end of yearday 148 when ΔT became positive. The wind speed and direction exhibited a diurnal land–sea variation throughout this period, with peak west-northwest winds of about 4–7 m s^{-1} tending to occur during the afternoon, and wind speed minimums of about 1 m s^{-1} tending to occur just before sunrise. The agreement between the bulk C_n^2 estimates and the scintillation values during this 8-day period is generally very good. The bulk estimates are significantly smaller than the scintillation measurements when ΔT approaches zero on yeardays 142 and 148. The bulk and scintillation C_n^2 values generally agree very well despite the strong diurnal wind variations and frequent offshore flows in the coastal location. It is believed that the bulk model should perform even better in the open ocean where conditions are generally more stationary and horizontally homogeneous and the wind/wave fields are more likely to be in equilibrium.

A time series plot for 14–18 September 1998 (yeardays 257–261) is presented in Fig. 10. Conditions were stable throughout this period, with ΔT values ranging between about 1° and 3.3°C. The winds were offshore from the northwest to west during virtually the entire period, and exhibited a strong diurnal cycle with afternoon maximums of 6–8 m s^{-1} and nighttime minimums of about 1–3 m s^{-1}. Here, ΔT is highly correlated with the wind speed, also exhibiting daytime maximums due to advection of warm air from the nearby land by the stronger daytime offshore winds. The bulk C_n^2 estimates are clearly higher than both the buoy turbulent and scintillation C_n^2 measurements and generally do not follow the trends in the scintillation and turbulence data. The sharp peaks in the bulk C_n^2 estimates associated with the daytime peak ΔT values were not exhibited in either the turbulent or scintillation C_n^2 measurements, indicating that in these conditions ΔT is a poor predictor of C_n^2. The direct turbulent C_n^2 values agree reasonably well with the scintillation measurements, especially during the periods with higher wind speeds and larger ΔT values. This may be due to smaller finite sampling errors in the turbulence measurements with higher wind speeds (e.g., Wyngaard 1973), or to an improved signal-to-noise ratio in the sonic anemometer measurements with stronger temperature fluctuations when ΔT and wind speed are large. These results demonstrate that the bulk C_n^2 model performs poorly in stable stratification, at least for the conditions of this study in a coastal region with persistent offshore winds.

Scintillation C_n^2 measurements from both the May–

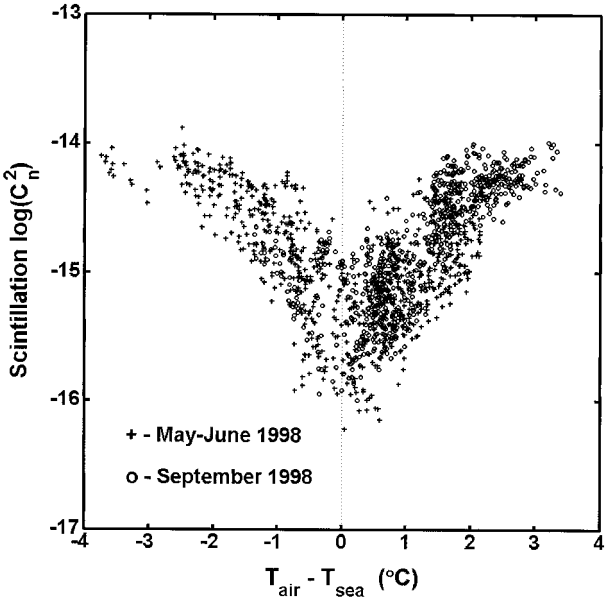

FIG. 11. Scintillation log(C_n^2) measurements versus air–sea temperature difference for the May–Jun 1998 experiment, indicated by crosses (+), and for the Sep 1998 experiment, indicated by circles (○).

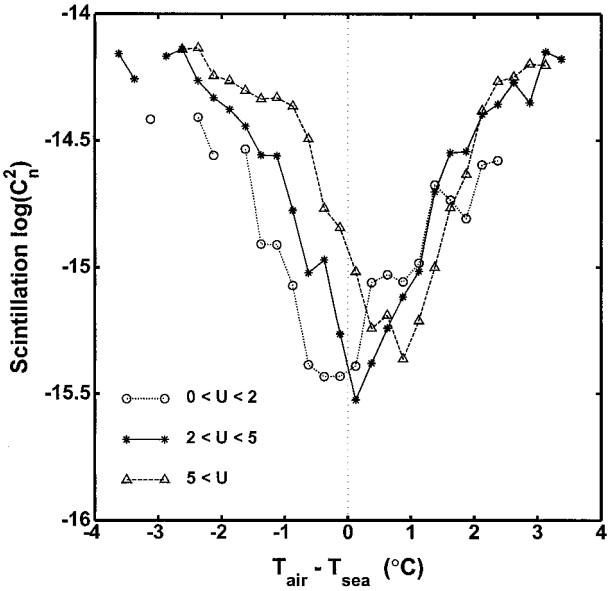

FIG. 12. Mean values of scintillation log(C_n^2) measurements for 0.25°C-wide ΔT bins and different wind speed ranges as indicated, vs the mean air–sea temperature difference. Data from both the May–Jun and Sep 1998 experiments are shown.

June and September 1998 experiments are plotted versus ΔT in Fig. 11. This plot clearly demonstrates that on average the scintillation-derived C_n^2 values increase with $|\Delta T|$, as qualitatively predicted by the bulk model. The minimum scintillation log(C_n^2) values measured during both experiments were slightly less than 1×10^{-16} and occurred when $|\Delta T| < 1$. While the measurements from the two experiments are similar for negative ΔT values, when $\Delta T > 0$ the May–June C_n^2 values on average are lower and exhibit more scatter than in September. The reason for this difference is not clear, but could be caused by the slightly higher wind speeds and lower relative humidity observed in May–June, which would lead to lower values of C_n^2 when $\Delta T > 0$, as qualitatively predicted by the bulk model

The scintillation log(C_n^2) values were averaged in ΔT bins of width 0.25°C and are plotted versus ΔT for different wind speed ranges in Fig. 12, for different relative humidity ranges in Fig. 13, and for different heights above the surface in Fig. 14. For a given ΔT, scintillation C_n^2 values generally increase with wind speed when ΔT is negative, and decrease with wind speed when ΔT is positive (see Fig. 12), as qualitatively predicted by the bulk model (see Fig. 2). In near-neutral conditions, when $|\Delta T| < \sim 1$°C, the values of ΔT where the minimum scintillation C_n^2 values occur become larger as the wind speed increases. This last pattern is not predicted by the bulk model and its cause is not understood at this time. For a given ΔT, C_n^2 generally decreases with relative humidity when ΔT is negative, and increases with relative humidity when ΔT is positive (see Fig. 13), again as qualitatively predicted by the bulk model (see Fig. 3). The height above the surface where the infrared rays passed varied with the tide level, providing an opportunity to study the height dependence of scintillation C_n^2 measurements. From Fig. 14 it is apparent that the scintillation C_n^2 measurements generally decreased with height as predicted. These results demonstrate that the bulk model correctly describes the qualitative effects of

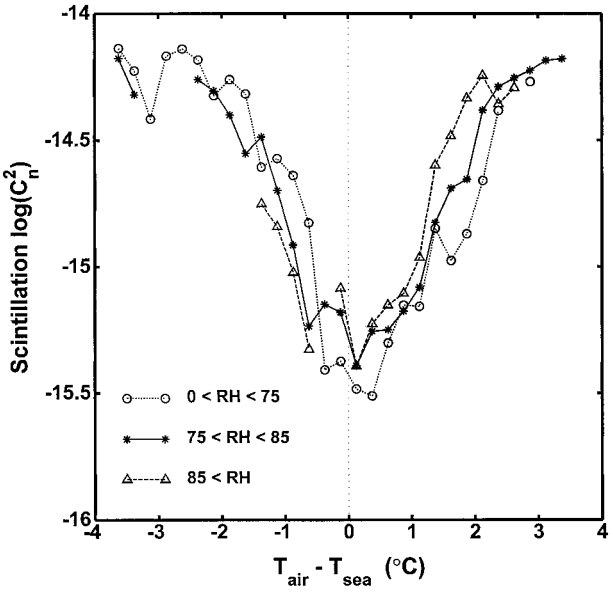

FIG. 13. Mean values of scintillation log(C_n^2) measurements for 0.25°C-wide ΔT bins and different relative humidity ranges as indicated, vs the mean air–sea temperature difference. Data from both the May–Jun and Sep 1998 experiments are shown.

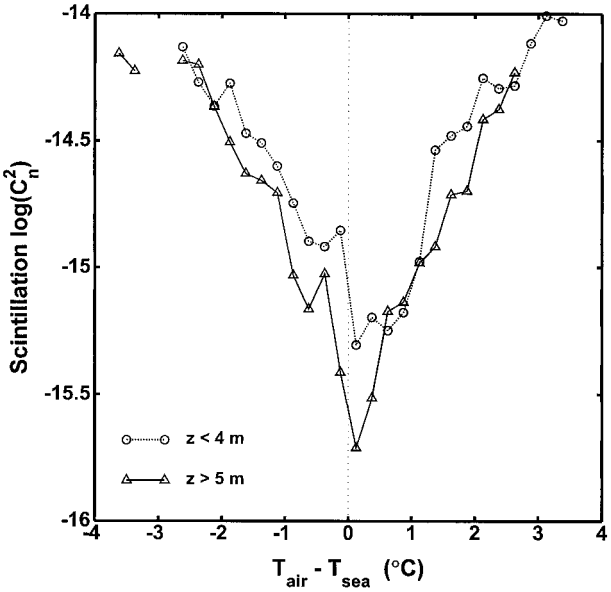

FIG. 14. Mean values of scintillation log(C_n^2) measurements for 0.25°C-wide ΔT bins and different heights above the surface as indicated, vs the mean air–sea temperature difference. Data from both the May–Jun and Sep 1998 experiments are shown.

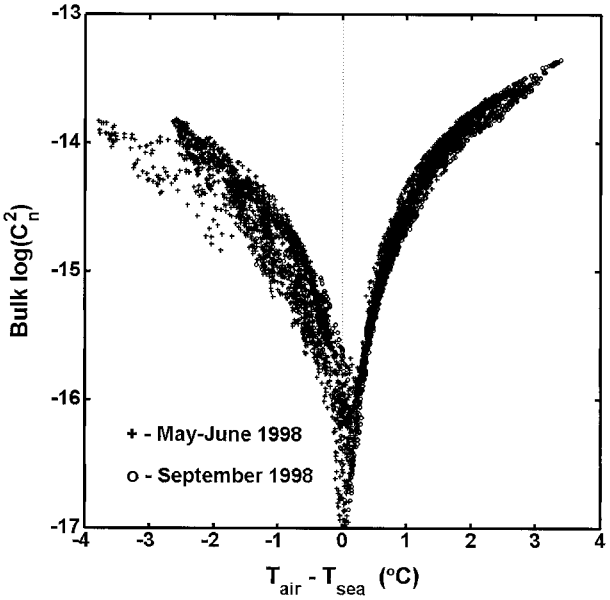

FIG. 15. Bulk log(C_n^2) estimates vs air–sea temperature difference for the May–Jun 1998 experiment, indicated by crosses (+), and for the Sep 1998 experiment, indicated by circles (○).

some of the processes that determine scintillation-derived C_n^2 values near the ocean surface.

The bulk C_n^2 estimates are plotted versus ΔT in Fig. 15. For a given ΔT the bulk data exhibit much less variation than the scintillation C_n^2 values (compare with Fig. 11), especially for positive ΔT values. The scintillation C_n^2 measurements most likely exhibit more variation than the bulk C_n^2 estimates because of differences inherent to path-averaged optical turbulence and mean single-point measurements and also because of processes that are not taken into account by the bulk model, as discussed previously in section 4. The bulk C_n^2 estimates drop rapidly as ΔT approaches small positive values, and reach much lower values than observed in the scintillation measurements.

In Fig. 16 the difference between the bulk and scintillation log(C_n^2) values are plotted versus ΔT. The bulk C_n^2 estimates for $\Delta T < -1$°C exhibit very good agreement with the scintillation C_n^2 measurements, although the bulk estimates are slightly higher on average. As $|\Delta T|$ approaches small positive values, the bulk C_n^2 estimates from both experiments become increasingly smaller than the scintillation measurements, by over two orders of magnitude in some cases. Tunick (1998) reported a similar finding for a bulk model based on mean temperature and humidity gradient measurements over land. For increasing ΔT values greater than about 1°C, the bulk C_n^2 estimates become increasingly larger than the scintillation measurements. This is especially true for the May–June dataset, in which the bulk C_n^2 estimates are on average an order of magnitude larger than the scintillation measurements for $\Delta T \approx 2$°C.

In Fig. 17 the difference between bulk estimates and direct turbulent measurements of C_T^2 from the buoy are plotted versus ΔT for the September 1998 experiment. Similar to the bulk-scintillation C_n^2 comparison in Fig. 16, the bulk C_T^2 estimates become increasingly smaller than the turbulence measurements as ΔT approaches zero, and in stable conditions the bulk C_T^2 estimates

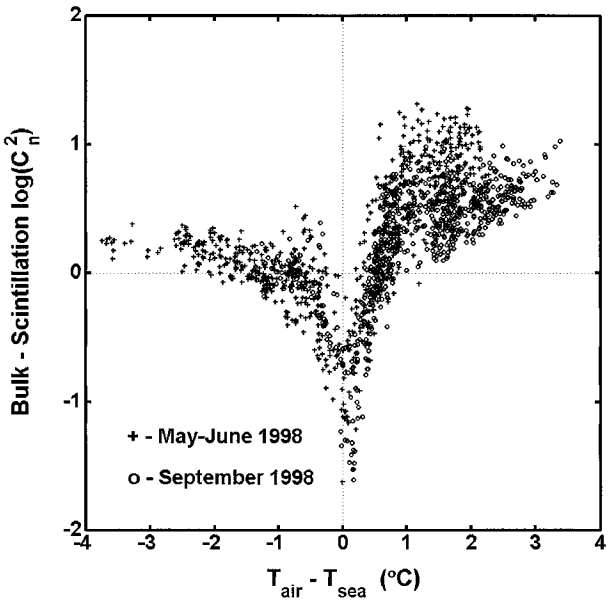

FIG. 16. Bulk log(C_n^2) − scintillation log(C_n^2) values vs air–sea temperature difference for the May–Jun 1998 experiment, indicated by crosses (+), and for the Sep 1998 experiment, indicated by circles (○).

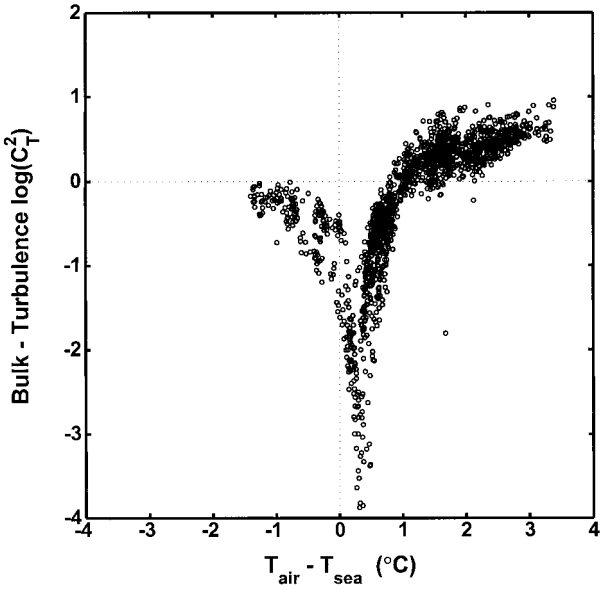

FIG. 17. Bulk $\log(C_T^2)$ − turbulent $\log(C_T^2)$ values vs air–sea temperature difference for the Sep 1998 experiment.

become increasingly larger than the turbulence values as ΔT increases. This result indicates that the observed differences between scintillation and bulk structure parameters in near-neutral and stable conditions are most likely due to deficiencies in the bulk model in such conditions and not just to differences between mean single-point environmental measurements and path-averaged scintillation measurements. Possible explanations for such deficiencies in the bulk model are discussed in the next section.

7. Conclusions

The results presented above demonstrate that in unstable conditions (negative air–sea temperature differences) scintillation-derived C_n^2 values can be estimated over the ocean with good accuracy from mean meteorological measurements using bulk methods. In stable conditions (positive air–sea temperature differences), on the other hand, the bulk C_n^2 estimates did not agree well with either the scintillation or direct turbulent-measured C_n^2 values. These results are probably due to the fact that MOS theory in general has been found to describe the dynamic characteristics of unstable surface layers better than it does stable surface layers. This is evident in the observation that the MOS stability functions (including the dimensionless structure parameter functions f_T, f_q, and f_{Tq}, upon which the bulk C_n^2 model depends) have been determined with greater certainty in unstable conditions than in stable conditions. Specific reasons why the MOS-based bulk model did not perform as well in stable conditions may include the following:

1) The thermal stratification in very stable conditions suppresses vertical mixing that can allow the atmosphere to become effectively decoupled from the surface, thereby violating the MOS assumption that the turbulent fluxes are constant with height.
2) In very stable conditions the surface layer can become very thin and the measurement height and/or the height where the bulk C_n^2 value was computed may be above the constant flux layer in a region where MOS scaling is not valid.
3) Surface heterogeneity, which is expected in a coastal ocean region, especially in offshore flow, has a much greater impact on atmospheric turbulence in stable conditions (e.g., Horst and Weil 1994; Mahrt 1999) and will invalidate MOS theory if the dynamic atmospheric properties depend upon surface characteristics.
4) Measurement of turbulent fluxes in stable surface layers characterized by weak, intermittent turbulence is very difficult, leading to large uncertainties in the stable MOS functions used in the bulk C_n^2 model (Mahrt 1999).

The bulk-scintillation C_n^2 and bulk-turbulent C_T^2 comparisons demonstrated that in stable conditions bulk scalar structure parameter estimates on average become increasingly *higher* than both path-averaged scintillation and single-point turbulence measurements as ΔT increases. A possible cause of this deviation is the modification of near-surface atmospheric vertical gradients by ocean waves. The infrared rays in this experiment pass only about 3–5 m above the surface at the midpoint of the path, depending upon tide and wave conditions, which is almost certainly within the wave boundary layer (WBL). Theoretical studies and observations have shown that vertical mixing within the WBL is enhanced by ocean waves (Hare et al. 1997). We believe that surface wave enhancement of atmospheric mixing would be greatest in stable conditions. In unstable conditions the stratification promotes vertical motions, therefore the wave-induced mixing would most likely be negligible in comparison with the relatively strong mixing already present. Conversely, in stable conditions the stratification suppresses vertical motions, therefore the forced wave-induced mixing of the lower atmosphere could be significant when compared with the weak turbulent mixing present. Enhanced wave-induced mixing would decrease the actual vertical temperature and humidity gradients from the traditional MOS-predicted forms for stable conditions, which would lead to bulk C_n^2 and C_T^2 estimates that are too high.

The bulk-scintillation C_n^2 and bulk-turbulent C_T^2 comparisons also demonstrated that in near-neutral conditions the bulk structure parameter estimates become much lower than both the scintillation and turbulence measurements as ΔT approaches zero. The probable reason for this result is that the *instantaneous* air–sea difference at the measurement height actually fluctuates between slightly positive and negative values, leading to a near-zero *mean* air–sea difference measurement and

thus a near-zero bulk structure parameter estimate. However, in the presence of atmospheric turbulence the nonzero instantaneous scalar gradients could lead to significant scalar fluctuations and much larger actual structure parameter values than predicted by the bulk model. This situation could be caused by such factors as vertically varying horizontal advection, time-varying vertical transport from above, or ocean wave influences on the near-surface scalar gradients. These results indicate that current bulk methods for estimating scalar structure parameters based on mean air–sea differences will underestimate the structure parameter when the measured mean air–sea difference approaches zero.

Last, it should be noted that the results of this study were obtained in a coastal region and it is probable that the bulk model will perform better in the open ocean where conditions are more likely to be stationary and horizontally homogeneous and the surface wave field is more likely to reach fully developed equilibrium states. The authors believe that the most promising means toward improving near-surface bulk C_n^2 models is to obtain a better understanding of the MOS functions over the ocean for a wide range of stability conditions, and particularly of the role of ocean waves in modifying near-surface vertical gradients and turbulence characteristics.

Acknowledgments. This work was funded by the U.S. Office of Naval Research under the EOPACE program, with Drs. Scott Sandgathe and Ronald Ferek as managers. The authors thank Mr. Keith Jones (Naval Postgraduate School) and Mr. Doug McKinney (McKinney Technology, Inc.) for their efforts in building and deploying the research buoy and Mr. William Moision and Dr. Stephen Hammel for their assistance in acquiring and analyzing the scintillation data. A special thanks is due to Dr. Douglas Jensen for his able organizational skills during EOPACE.

APPENDIX

Dimensionless Profile Functions

The commonly used ''Businger–Dyer'' forms for the integrated dimensionless profile functions for wind speed, Ψ_U, and potential temperature, Ψ_θ, in unstable conditions ($\xi < 0$) are given by (Paulson 1970)

$$\Psi_U(\xi) = 2\ln\left[\frac{1 + \Phi_U^{-1}(\xi)}{2}\right] + \ln\left[\frac{1 + \Phi_U^{-2}(\xi)}{2}\right] - 2\arctan[\Phi_U^{-1}(\xi)] + \frac{\pi}{2} \quad \text{and} \tag{A1}$$

$$\Psi_\theta(\xi) = 2\ln\left[\frac{1 + \Phi_\theta^{-1}(\xi)}{2}\right], \tag{A2}$$

where

$$\Phi_U(\xi) = (1 - 20\xi)^{-1/4} \quad \text{and} \tag{A3}$$

$$\Phi_\theta(\xi) = (1 - 16\xi)^{-1/2}. \tag{A4}$$

These functions have been well verified by experimental data obtained over land over the stability range $-2 \le \xi \le 0$ (Hogstrom 1996). In this study we follow the usual assumption that $\Psi_q = \Psi_\theta$.

Asymptotic scaling (Wyngaard 1973) and over-land measurements (e.g., Carl et al. 1973; Holtslag 1984) indicate that in very unstable conditions approaching the free-convective limit (i.e., $\xi \to -\infty$), Φ_U, Φ_θ, and Φ_q should exhibit a $\xi^{-1/3}$ dependence, as follows:

$$\Phi_c(\xi) = (1 - 16\xi)^{-1/3}, \tag{A5}$$

where the subscript c denotes the free-convective limit. The integrated form of Φ_c is given by

$$\Psi_c(\xi) = \frac{3}{2}\ln\left(\frac{\Phi_c^{-2} + \Phi_c^{-1} + 1}{3}\right) - \sqrt{3}\arctan\left(\frac{2\Phi_c^{-1} + 1}{\sqrt{3}}\right) + \frac{\pi}{\sqrt{3}}. \tag{A6}$$

Because (A5) has been observed to fit wind speed and temperature profile observations better than (A3) and (A4) under highly unstable conditions, we follow Fairall et al. (1996) in ''blending'' the Businger–Dyer (Ψ_{BD}) equations given in (A1) and (A2) and the ''free-convective'' (Ψ_c) form for Ψ using the equation

$$\Psi = \chi\Psi_{BD} + (1 - \chi)\Psi_c, \tag{A7}$$

where

$$\chi = \frac{1}{1 + \xi^2/40}. \tag{A8}$$

This blending function χ has been slightly modified from the form used by Fairall et al. (1996) to enable Ψ_U and Ψ_θ to more closely match (A1) and (A2) over the interval $-2 \le \xi \le 0$, where they have been well verified by experimental data.

For stable conditions we use the functions given by Beljaars and Holtslag (1991) for Ψ_U and Ψ_θ, as follows:

$$\Psi_U = -a\xi - b\left(\xi - \frac{c}{d}\right)\exp(-d\xi) - \frac{bc}{d}, \quad \xi > 0 \tag{A9}$$

and

$$\Psi_\theta = 1 - \left(1 + \frac{2a}{3}\xi\right)^{3/2} - b\left(\xi - \frac{c}{d}\right)\exp(-d\xi) - \frac{bc}{d}, \quad \xi > 0 \tag{A10}$$

where $a = 1$, $b = \frac{2}{3}$, $c = 5$, and $d = 0.35$.

REFERENCES

Anctil, F., and M. A. Donelan, 1996: Air–water momentum flux observations over shoaling waves. *J. Phys. Oceanogr.,* **26,** 1344–1353.

Andreas, E. L., 1987: On the Kolmogorov constants for the temperature–humidity cospectrum and the refractive index spectrum. *J. Atmos. Sci.,* **44,** 2399–2406.

——, 1988: Estimating C_n^2 over snow and ice from meteorological data. *J. Opt. Soc. Amer.,* **5A,** 481–495.

——, R. J. Hill, J. R. Gosz, D. I. Moore, W. D. Otto, and A. D. Sarma, 1998: Statistics of surface-layer turbulence over terrain with metre-scale heterogeneity. *Bound.-Layer Meteor.,* **86,** 379–408.

Beljaars, A. C. M., and A. A. M. Holtslag, 1991: Flux parameterization over land surfaces for atmospheric models. *J. Appl. Meteor.,* **30,** 327–341.

Carl, D. M., T. C. Tarbell, and H. A. Panofsky, 1973: Profiles of wind and temperature from towers over homogeneous terrain. *J. Atmos. Sci.,* **30,** 788–794.

Churnside, J. H., 1993: Optical remote sensing. *Wave Propagation in Random Media (Scintillation),* V. I. Tatarskii, A. Ishimaru, and V. U. Zavorotny, Eds., SPIE Press and Institute of Physics Publishing, 235–245.

——, R. J. Lataitis, and J. J. Wilson, 1992: Two-color correlation of atmospheric scintillation. *Appl. Opt.,* **31,** 4285–4290.

Claverie, J., Y. Hurtaud, Y. de Fromont, and A. Junchat, 1995: Modelisation des profils verticaux d'indice de refraction et de C_n^2 en atmosphere marine. Proc. Propagation Assessment in Coastal Environments, NASA Tech. Rep. AGARD-CP-567, 29-1–29-11. [Available from NASA Center for Aerospace Information, 800 Elkridge Landing Rd., Linthicum Heights, MD 21090-2934.]

Davidson, K. L., G. E. Schacher, C. W. Fairall, and A. K. Goroch, 1981: Verification of the bulk method for calculating overwater optical turbulence. *Appl. Opt.,* **20,** 2919–2924.

Edson, J. B., and C. W. Fairall, 1998: Similarity relationships in the marine atmospheric surface layer for terms in the TKE and scalar variance budgets. *J. Atmos. Sci.,* **55,** 2311–2328.

——, ——, P. G. Mestayer, and S. E. Larsen, 1991: A study of the inertial-dissipation method for computing air–sea fluxes. *J. Geophys. Res.,* **96,** 10 689–10 711.

Fairall, C. W., G. E. Schacher, and K. L. Davidson, 1980: Measurements of the humidity structure function parameters, C_q^2 and C_{Tq}, over the ocean. *Bound.-Layer Meteor.,* **19,** 81–92.

——, E. F. Bradley, D. P. Rogers, J. B. Edson, and G. S. Young, 1996: Bulk parameterization of air–sea fluxes for Tropical Ocean–Global Atmosphere Coupled–Ocean Atmosphere Response Experiment. *J. Geophys. Res.,* **101,** 3747–3764.

——, A. B. White, J. B. Edson, and J. E. Hare, 1997: Integrated shipboard measurements of the marine boundary layer. *J. Atmos. Oceanic Technol.,* **14,** 338–359.

Forand, J. L., 1999: The L(W)WKD marine boundary layer model version 7.09. Defence Research Establishment, Valcartier Rep. DREV-TR-1999-099, 94 pp. [Available from Director Research and Development Communications and Information Management, Department of National Defence, Ottawa, ON K1A 0K2, Canada.]

Friehe, C. A., 1977: Estimation of the refractive-index temperature structure parameter over the ocean. *Appl. Opt.,* **16,** 334–340.

Hare, J. E., T. Hara, J. B. Edson, and J. M. Wilczak, 1997: A similarity analysis of the structure of airflow over surface waves. *J. Phys. Oceanogr.,* **27,** 1018–1037.

Hill, R. J., 1989: Implications of Monin–Obukhov similarity theory for scalar quantities. *J. Atmos. Sci.,* **46,** 2236–2244.

——, and S. F. Clifford, 1978: Modified spectrum of atmospheric temperature fluctuations and its application to optical propagation. *J. Opt. Soc. Amer.,* **68,** 892–899.

Hogstrom, U., 1996: Review of some basic characteristics of the atmospheric surface layer. *Bound.-Layer Meteor.,* **78,** 215–246.

Holtslag, A. A. M., 1984: Estimates of diabatic wind speed profiles from near-surface weather observations. *Bound.-Layer Meteor.,* **29,** 225–250.

Horst, T. W., and J. C. Weil, 1994: How far is far enough?: The fetch requirements for micrometeorological measurement of surface fluxes. *J. Atmos. Oceanic Technol.,* **11,** 1018–1025.

Kohsiek, W., 1982: Measuring C_T^2, C_Q^2 and C_{TQ} in the unstable surface layer, and relations to the vertical fluxes of heat and moisture. *Bound.-Layer Meteor.,* **24,** 89–107.

Kunz, G. J., M. M. Moerman, P. J. Fritz, and G. de Leeuw, 1996: Validation of a bulk turbulence model with thermal images of a point source. *Proc. SPIE,* **2828,** 108–116.

Liu, W. T., K. B. Katsaros, and J. B. Businger, 1979: Bulk parameterization of air–sea exchanges of heat and water vapor including the molecular constraints at the interface. *J. Atmos. Sci.,* **36,** 1722–1735.

Mahrt, L., 1999: Stratified atmospheric boundary layers. *Bound.-Layer Meteor.,* **90,** 375–396.

——, D. Vickers, J. Edson, J. Sun, J. Hojstrup, J. Hare, and J. M. Wilczak, 1998: Heat flux in the coastal zone. *Bound.-Layer Meteor.,* **86,** 421–446.

Paulson, C. A., 1970: The mathematical representation of wind speed and temperature profiles in the unstable atmospheric surface layer. *J. Appl. Meteor.,* **9,** 857–861.

Sadot, D., and N. S. Kopeika, 1992: Forecasting optical turbulence strength on the basis of macroscale meteorology and aerosols: Models and validation. *Opt. Eng.,* **31,** 200–212.

Tunick, A. D., 1998: The refractive index structure parameter/atmospheric optical turbulence model: CN2. U.S. Army Research Laboratory Rep. ARL-TR-1615, 27 pp. [Available from U.S. Army Research Laboratory, 2800 Powder Mill Rd., Adelphi, MD 20783-1197.]

Vickers, D., and L. Mahrt, 1997: Fetch limited drag coefficients. *Bound.-Layer Meteor.,* **85,** 53–79.

——, and ——, 1999: Monin–Obukhov similarity theory in the coastal zone. Preprints, *13th Symp. on Boundary Layers and Turbulence,* Dallas, TX, Amer. Meteor. Soc., 407–410.

Wang, T., G. R. Ochs, and S. F. Clifford, 1978: A saturation-resistant optical scintillometer to measure C_n^2. *J. Opt. Soc. Amer.,* **68,** 334–338.

Wu, J., 1980: Wind-stress coefficients over sea surface near neutral conditions—A revisit. *J. Phys. Oceanogr.,* **10,** 727–740.

Wyngaard, J. C., 1973: On surface-layer turbulence. *Workshop on Micrometeorology,* D. A. Haugen, Ed., Amer. Meteor. Soc., 101–149.